Journal of Magnetic Resonance 349 (2023) 107412

Contents lists available at ScienceDirect

Journal of Magnetic Resonance

journal homepage: www.elsevier.com/locate/jmr

Sometimes pulses just have to be perfect – An example based on the measurement of amide proton transverse relaxation rates in proteins

Atul Kaushik Rangadurai [a,b,c,d,*,2], Yuki Toyama [a,b,c,*,1,2], Lewis E. Kay [a,b,c,d,*]

[a] Department of Molecular Genetics, University of Toronto, Toronto, Ontario M5S 1A8, Canada
[b] Department of Biochemistry, University of Toronto, Toronto, Ontario M5S 1A8, Canada
[c] Department of Chemistry, University of Toronto, Toronto, Ontario M5S 1A8, Canada
[d] Hospital for Sick Children, Program in Molecular Medicine, 555 University Avenue, Toronto, Ontario M5G 1X8, Canada

ARTICLE INFO

Article history:
Received 18 January 2023
Revised 17 February 2023
Accepted 19 February 2023
Available online 2 March 2023

Keywords:
$^1H^N$ transverse relaxation
Pulse imperfections
Multiple quantum coherences
Cross-correlated relaxation

ABSTRACT

The measurement of spin relaxation rates provides a unique avenue for quantifying dynamic processes in biomolecules. In order to simplify analysis of the measurements so that a few key intuitive parameters can be extracted, it is often the case that experiments are designed to eliminate interference effects between different classes of spin relaxation. One example emerges in the measurement of amide proton ($^1H^N$) transverse relaxation rates in ^{15}N labeled proteins, where ^{15}N inversion pulses are applied during a relaxation element to eliminate cross-correlated spin relaxation between $^1H^N$-^{15}N dipole-$^1H^N$ CSA interactions. We show that unless these pulses are essentially perfect, significant oscillations in magnetization decay profiles can be obtained, due to the excitation of multiple-quantum coherences, leading potentially to errors in measured R_2 rates. With the recent development of experiments for quantifying electrostatic potentials via amide proton relaxation rates, the need for highly accurate measurement schemes becomes critical. Straightforward modifications to existing pulse sequences are suggested to achieve this goal.

1. Introduction

NMR spectroscopy has emerged as a powerful analytical tool to probe a wide range of properties of biological molecules, including those that relate to both structure and dynamics [1,2]. Central to the growth of the number of applications has been the concomitant increase in the available repertoire of pulse sequences that are designed to precisely manipulate magnetization to extract the desired molecular property. Artifacts that arise from imperfections in the manipulations, such as those resulting from radio frequency (rf) pulse offsets and inhomogeneity effects, or pulse miscalibrations, are often eliminated through phase cycling [3], the application of pulsed field gradients [4], the use of pulses that are broadbanded and highly tolerant to rf inhomogeneity [5–8], or a combination of all three approaches. In many cases these residual imperfections do not significantly impede the extraction of the information of interest (for example in resonance assignment spectra), although they can affect the sensitivity of the resulting spectra [9], while in other applications quantitation can potentially be compromised.

One such example of the latter situation emerged in our initial attempts to quantify near surface electrostatic potentials (ϕ_{ENS}) in proteins based on the measurement of backbone amide ^1H ($^1H^N$) transverse relaxation rates in a series of samples in which differently charged paramagnetic co-solutes are added. As described in an elegant series of papers by Iwahara and coworkers [10–12], ratios of paramagnetic relaxation enhancement (PRE) rates obtained from the different co-solutes can be recast in terms of ϕ_{ENS} values. A number of different approaches for measurement of $^1H^N$ PREs are possible, including those that record decay rates during free-precession evolution of $^1H^N$ TROSY magnetization or during a relaxation period where the full complement of magnetization is used (*i.e.*, non-TROSY), with interconversion between TROSY and anti-TROSY components achieved in this case via application of ^{15}N inversion pulses to ensure the exponential decay of magnetization [13,14]. Alternative schemes based on measurement of $^1H^N$ $R_{1\rho}$ rates are also possible [15]. Although the TROSY based scheme is clearly advantageous for applications involving

* Corresponding authors at: Department of Molecular Genetics, University of Toronto, Toronto, Ontario M5S 1A8, Canada.
E-mail addresses: atulkaushik.rangadurai@sickkids.ca (A.K. Rangadurai), yuki.toyama@utoronto.ca, yuki.toyama@riken.jp (Y. Toyama), kay@pound.med.utoronto.ca (L.E. Kay).
[1] Present address: Center for Biosystems Dynamics Research, RIKEN, Kanagawa 230-0045, Japan.
[2] Equal contributions.

https://doi.org/10.1016/j.jmr.2023.107412
1090-7807/

large protein systems, and we have used it in relaxation studies of intrinsically disordered proteins in highly viscous phase-separated samples [16], there are many applications involving relatively small proteins dissolved in buffer where non-TROSY methods are preferred. In this regard, one such experiment was proposed by our laboratory over two decades ago in which a transverse relaxation element preceded the recording of ^{15}N and ^{1}H^{N} chemical shifts using a simple HSQC-based pulse scheme [13]. Spectra in this application were recorded on ubiquitin at 500 MHz using a spectrometer with a room temperature probe. Viewed from the more critical and much more sensitive lens of a 1 GHz spectrometer, where resonance offset effects can be especially significant, it became clear that many of the relaxation decay profiles recorded on a concentrated sample (~3 mM) of a highly deuterated 7.5 kDa domain of protein L using the same pulse sequence were artifactual. Artifacts were also observed in applications involving much more dilute, protonated samples, as well.

Herein, we establish that the source of these artifacts lies in the ^{15}N pulses that are used to refocus cross-correlated spin relaxation during the relaxation element that is varied in a set of 2D ^{15}N-^{1}H^{N} correlation experiments to measure site-specific ^{1}H^{N} R_2 rates [13], and that inversion profiles that are essentially perfect are required to obtain exponential magnetization decay profiles. A number of such (near) perfect pulses are presented. Our results serve as a stark reminder (at least to us) of the importance of the selection of optimal pulses in applications that can be sensitive to pulse imperfections, and that careful thought as to which pulses in a sequence are particularly an issue in this regard can, potentially, significantly increase the robustness of the resulting data.

2. Materials and methods

2.1. Sample preparation

A [U-^{15}N,^{2}H]-labeled protein L sample (~3 mM) dissolved in 50 mM sodium phosphate, 0.05% NaN_3, 10% D_2O buffer (pH 6.0) was prepared as described previously [17]. A standard 5 mm sample tube was used.

2.2. NMR measurements

NMR measurements were performed at 23.5 Tesla (1 GHz ^{1}H frequency) using a Bruker AVANCE NEO spectrometer equipped with a helium-cooled *x*, *y*, *z* pulsed-field gradient triple-resonance probe or at 11.7 Tesla (500 MHz ^{1}H frequency) on a Bruker AVANCE III HD spectrometer equipped with a liquid nitrogen-cooled *z* pulsed-field gradient triple-resonance probe. All spectra were processed and analyzed using the NMRPipe suite of programs [18]. Peak intensities were extracted by using the Peakipy software package (https://github.com/j-brady/peakipy).

^{1}H^{N} R_2 relaxation measurements of protein L were performed using an HSQC-based pulse sequence adapted from that described by Donaldson et al. [13] that is equally applicable for studies of deuterated or protonated proteins. A schematic of the initial part of the experiment is highlighted in Fig. 1A, where the relaxation of transverse ^{1}H^{N} magnetization occurs during a relaxation interval of T and in-phase ^{1}H^{N} magnetization evolves subject to the one-bond ^{1}H^{N}-^{15}N scalar coupling for a period of $\delta \sim 1/2J_{HN}$ to generate anti-phase ^{1}H^{N} magnetization for subsequent transfer to ^{15}N (*i.e.*, HSQC part of the sequence). An amide ^{1}H-selective REBURP pulse [19] (bandwidth of 2.8 ppm centered at 7.95 ppm, 1.36 ms at 1 GHz) is applied in the middle of the relaxation period (T) to refocus homonuclear J coupled evolution involving ^{1}H^{N} and aliphatic proton spins (in the case of protonated proteins), and so as not to perturb water magnetization. Water selective SEDUCE pulses [20] (1.8 ms) were applied to maintain water magnetization along the *z*-axis during the relaxation period and to ensure that water resides along the *z*-axis at the completion of each scan [21], as illustrated in the timing diagram of the original sequence [13]. There, low-power rectangular pulses were used in place of SEDUCE pulses; there is little difference between what shape is used however, so long as the chosen pulses minimize excitation of amide protons that otherwise would affect the sensitivity of the experiment. In this regard, we prefer the SEDUCE-based scheme. ^{15}N decoupling during acquisition was achieved using a 1.3 kHz (1 GHz) or 1 kHz (500 MHz) WALTZ-16 [22] field. A number of different types of ^{15}N inversion pulses were applied during the relaxation period to remove cross-correlated relaxation interference between ^{1}H^{N}-^{15}N dipole–dipole and ^{1}H^{N} CSA interactions. These included, adiabatic pulses [7] (1 ms, 5 kHz maximum rf intensity and a 40 kHz sweep about 119 ppm; code to generate pulses is available online as described in the data availability statement), 180° rectangular pulses, $90°_x$-$180°_y$-$90°_x$ composite pulses [23], and $90°_x$-$240°_y$-$90°_x$ composite pulses [24], the latter three of which were applied at the highest rf field strength possible (typically ~ 6 kHz). Twenty-two relaxation times (from 5 ms to 62.25 ms, with all relaxation delays sampled prior to incrementing t_1) to quantify ^{1}H^{N} R_2 values were used in all cases, along with a recovery delay of 1.5 s, a spectral width of 21 ppm in the indirect dimension corresponding to an acquisition time of 25 ms, along with either 2 (1 GHz) or 4 (500 MHz) scans/FID to give net acquisition times of ~2 h/data set. All the measurements were performed at 25 °C.

^{1}H^{N} R_2 values were obtained by fitting the decay curves to a simple exponential function, $y = y_o \exp(-R_2T)$, where T is the parametrically varied relaxation delay, as shown in Fig. 1A. Note that the durations of ^{15}N pulses applied during the relaxation element do not need to be taken into account in the fit as they are constant for each value of T. Simulations of the effect of the ^{1}H^{N} REBURP pulse (applied along ± *x*), including relaxation, establish that there is a negligible difference if the starting ^{1}H^{N} magnetization is along *x* or along *y*. Thus, as for the ^{15}N pulses, the ^{1}H^{N} pulse contributes to the length of the relaxation period, but its effect is independent of T so that it does not need to be included to extract accurate R_2 values from fits of the relaxation decays.

2.3. Numerical simulations

Decay curves of ^{1}H^{N} in-phase transverse magnetization (H_x) and the trajectories of ^{1}H^{N} in-phase, ^{1}H^{N} anti-phase ($2H_yN_z$), and ^{1}H^{N}-^{15}N multiple quantum elements ($2H_yN_x$ and $2H_yN_y$) were simulated by calculating the time evolution of the density matrix of an isolated ^{1}H^{N}-^{15}N J-coupled two spin spin-system in Liouville space, as described by Allard *et al.* [25]. The operative Hamiltonian at time t, $\widehat{\mathscr{H}}(t)$, is defined by,

$$\widehat{\mathscr{H}}(t) = \Omega_N N_z + \pi J_{HN} 2H_z N_z + \omega_{1,H}(t) I_x + \omega_{1,N}(t)\cos(\phi_N(t)) \times N_x + \omega_{1,N}(t)\sin(\phi_N(t)) N_y \quad (1)$$

where Ω_N is the offset of the ^{15}N spin from the ^{15}N carrier in rad/s, J_{HN} is the ^{1}H^{N}-^{15}N J-coupling constant (=90 Hz in the simulations), $\omega_{1,H}(t)$ and $\omega_{1,N}(t)$ (rad/s) are the radio frequency field strengths for ^{1}H^{N} and ^{15}N, respectively, at time t, and $\phi_N(t)$ is the phase of the ^{15}N radio frequency field during application of the nitrogen pulse. It was assumed that the ^{1}H carrier was on-resonance unless otherwise mentioned. The time evolution of the density matrix, $\sigma(t)$, during the simulations considered in the text was calculated by numerically propagating $\sigma(t)$ using a small time step, Δt, via

$$\sigma(t+\Delta t) = \exp\left\{-\left(i\widehat{\widehat{\mathscr{L}}}(t) + \widehat{\widehat{\Gamma}}\right)\Delta t\right\}\sigma(t) \quad (2)$$

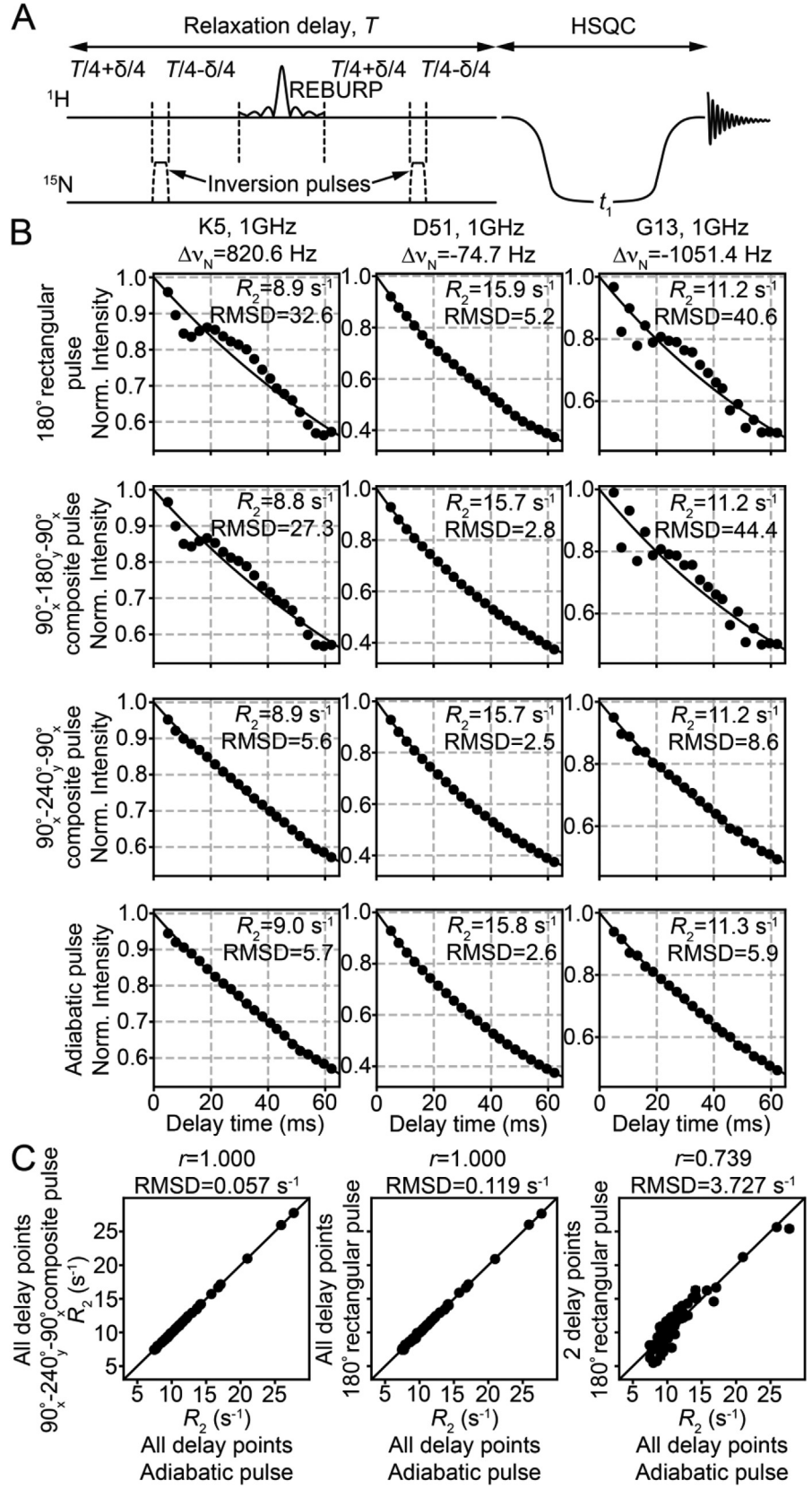
A
Relaxation delay, T
HSQC
T/4+δ/4
T/4-δ/4
T/4+δ/4
T/4-δ/4
REBURP
1H
15N
Inversion pulses
t1
B
K5, 1GHz
Δν_N=820.6 Hz
D51, 1GHz
Δν_N=-74.7 Hz
G13, 1GHz
Δν_N=-1051.4 Hz
180° rectangular pulse
Norm. Intensity
R2=8.9 s-1
RMSD=32.6
R2=15.9 s-1
RMSD=5.2
R2=11.2 s-1
RMSD=40.6
90°x-180°y-90°x composite pulse
R2=8.8 s-1
RMSD=27.3
R2=15.7 s-1
RMSD=2.8
R2=11.2 s-1
RMSD=44.4
90°x-240°y-90°x composite pulse
R2=8.9 s-1
RMSD=5.6
R2=15.7 s-1
RMSD=2.5
R2=11.2 s-1
RMSD=8.6
Adiabatic pulse
R2=9.0 s-1
RMSD=5.7
R2=15.8 s-1
RMSD=2.6
R2=11.3 s-1
RMSD=5.9
Delay time (ms)
C
r=1.000
RMSD=0.057 s-1
r=1.000
RMSD=0.119 s-1
r=0.739
RMSD=3.727 s-1
All delay points
90°x-240°y-90°x composite pulse
R2 (s-1)
All delay points
180° rectangular pulse
2 delay points
180° rectangular pulse
R2 (s-1)
All delay points
Adiabatic pulse

where $\widehat{\mathscr{L}}(t)$ is a 15 × 15 Liouvillian matrix expressed using the Cartesian product operator bases (H_x, H_y, H_z, N_x, N_y, N_z, $2H_xN_z$, $2H_yN_z$, $2H_zN_x$, $2H_zN_y$, $2H_xN_x$, $2H_xN_y$, $2H_yN_x$, $2H_yN_y$, and $2H_zN_z$, not including the identity operator) at time t, and $\widehat{\hat{\Gamma}}$ is a relaxation matrix including auto- and cross-relaxation terms [25]. The initial condition $\sigma(0) = H_x$ was used, and Δt = 1 μs in all of the simulations. Each matrix component for $\widehat{\mathscr{L}}_{rs}(t)$ was calculated according to

$$\widehat{\mathscr{L}}_{rs}(t) = \frac{\left\langle r\left|\left[\widehat{\mathscr{H}}(t), s\right]\right\rangle\right.}{\langle r|r\rangle} \quad (3)$$

where |r> and |s> are density elements listed above. The value of $\omega_{1,H}(t)$ was set to 2π × 25000 (rad/s) for the ^{1}H refocusing pulse (square pulse in the simulations, but REBURP profile [19] in experiments), and $\omega_{1,N}(t)$ was set to 2π × 6250 (rad/s) for calculating the ^{15}N 180°$_x$ inversion and 90°$_x$-180°$_y$-90°$_x$/90°$_x$-240°$_y$-90°$_x$ composite inversion pulses. For the ^{15}N adiabatic refocusing scheme, the amplitude, $\omega_{1,N}(t)$, and the phase, $\phi_N(t)$, of the radio frequency field were changed in each time step of the 1 ms pulse, as described previously [7]. A maximum field strength of 2π × 5000 (rad/s) and a frequency sweep rate of 40 kHz/ms were used. The relaxation matrix, $\widehat{\hat{\Gamma}}$, includes terms for the ^{1}H^N-^{15}N dipole–dipole interaction (the distance between ^{1}H^N and ^{15}N nuclei, r_{HN} = 1.04 Å), ^{1}H^N and ^{15}N chemical shift anisotropy (CSA) interactions (axially symmetric ^{15}N and ^{1}H CSA tensors with $|\Delta\sigma_N|$ = 161 ppm and $|\Delta\sigma_H|$ = 9.9 ppm), and ^{1}H^N-^{15}N dipole–dipole/^{1}H^N or ^{15}N CSA cross-correlation terms, assuming a static magnetic field strength of 23.5 Tesla (1 GHz ^{1}H frequency). The CSA parameters used were average values for β-sheet residues [26]. A spectral density function for isotropic rotational motion, $J(\omega) = \frac{2}{5}\cdot\frac{\tau_c}{1+\omega^2\tau_c^2}$, was assumed, where the rotational correlation time τ_c was set to 5 ns. The spectral density for dipole–dipole/CSA cross-correlated relaxation was obtained by multiplying $J(\omega)$ by $(3\cos^2\beta-1)/2$ [27], where β is the angle between the CSA principal axis of the assumed axially symmetric CSA tensor and the ^{15}N-^{1}H^N bond vector (β = 19° and 7° was used for ^{15}N and ^{1}H^N CSA, respectively).

3. Results and discussion

Fig. 1A shows a schematic of one of the pulse schemes that we have used to record ^{1}H^N transverse relaxation rates in ^{15}N labeled proteins based on the approach of Donaldson et al. [13]. A detailed timing diagram for the experiment is given in Ref. [13]. Briefly, and as depicted in the figure, a pair of ^{15}N inversion pulses are applied during the relaxation period (T) in order to eliminate contributions from ^{1}H^N-^{15}N dipole–dipole/^{1}H^N CSA cross-correlated relaxation [28–30]. Additionally, a selective ^{1}H^N chemical shift refocusing pulse is applied in the center of T, which does not perturb the water magnetization, and refocuses evolution from ^{1}H^N-^{1}H scalar couplings when protonated proteins are studied. Finally, in addition to the relaxation delay T, an additional delay, δ, is included so that the in-phase ^{1}H^N magnetization at the start of the interval evolves due to the one-bond ^{1}H^N-^{15}N scalar coupling for a duration of $\delta \sim 1/2J_{HN}$ to generate anti-phase ^{1}H^N magnetization by the end of this period for subsequent transfer to ^{15}N and recording of ^{15}N chemical shift during t_1 [13].

Profiles of decay curves recorded using a number of different ^{15}N inversion pulses are illustrated in Fig. 1B, measured on a U-[^{2}H,^{15}N]-labeled sample of protein L at 1 GHz, with three residues highlighted. The inversion pulses include rectangular (180°), 90°$_x$-180°$_y$-90°$_x$ composite [23], and 90°$_x$-240°$_y$-90°$_x$ composite [24] pulses, all applied at the highest possible power, and an adiabatic [7] (1 ms, 5 kHz) pulse with a sweep rate of 40 kHz/ms. The profiles chosen in Fig. 1B are derived from residues with backbone ^{15}N chemical shifts (indicated above the top profiles) that are either far downfield (K5, $\Delta\nu_N$ = 820.6 Hz), close to on-resonance (D51, $\Delta\nu_N$ = −74.7 Hz), or far upfield (G13, $\Delta\nu_N$ = −1051.4 Hz) of the ^{15}N carrier (119 ppm). Notably, artifacts are not observed when the pulses are effectively on-resonance, (D51, center column), but noticeable deviations from exponential fits (solid lines) are seen in the case where ^{15}N inversion pulses are either rectangular or of the 90°$_x$-180°$_y$-90°$_x$ composite variety and offsets are large (K5 and G13). In contrast, 90°$_x$-240°$_y$-90°$_x$ composite or adiabatic pulses are far more forgiving of offset effects. Thus, the resulting decay profiles are exponential, and the agreement between ^{1}H^N R_2 rates obtained using either set of pulses is excellent (Fig. 1C, left, Pearson correlation coefficient r = 1, RMSD = 0.06 s^{-1}).

In general, deviations from exponential decays would be expected to lead to errors in fitted R_2 relaxation rates. Interestingly, however, for both K5 and G13 the fitted R_2 values were very similar, irrespective of the ^{15}N pulses used. In general, this trend was observed for all residues in the protein, and R_2 rates obtained in schemes using adiabatic or 180° rectangular ^{15}N pulses are also in excellent agreement (Fig. 1C, center, r = 1.0, RMSD = 0.12 s^{-1}). The quality of the correlation between R_2 rates in this case does depend on the sampling scheme and on the number of delay points, however, with the large number of points in the present case ensuring good agreement in relaxation rates. By means of illustration we have further analyzed the relaxation data for K5, D51, and G13 recorded with the four different ^{15}N pulses by randomly retaining only eight data points from the profiles illustrated in Fig. 1. Fig. S1 plots histograms of R_2 values generated by repeating this analysis 50,000 times, showing that a considerable range of relaxation rates can be obtained in cases where deviations from mono-exponential decay are substantial. Notably, the correlation between rates from experiments using 180° rectangular pulses and adiabatic ^{15}N pulses deteriorates significantly when using only two delay points for the dataset recorded with rectangular pulses, as illustrated in Fig. 1C right (r = 0.74, RMSD = 3.73 s^{-1}). Here relaxation rates obtained from analysis of the full profile using adiabatic pulses are compared with those obtained from time points of 5 ms and 16 ms from profiles generated with ^{15}N 180° rectangular pulses. When high quality data (*i.e.*, exponential profiles) are obtained, the sampling scheme is much less of an issue, as illustrated by a comparison similar to that in Fig. 1C right, but where R_2 values from 2 delay points measured using 90°$_x$-240°$_y$-90°$_x$

Fig. 1. ^{1}H^N R_2 profiles depend critically on the nature of the inversion pulses used to suppress cross-correlated relaxation interactions. (A) Schematic of the pulse sequence used to measure ^{1}H^N R_2 relaxation rates of ^{15}N labeled proteins [13]. Dashed boxes denote ^{15}N inversion pulses that are applied during the relaxation period to refocus cross-correlated spin-relaxation between ^{1}H^N-^{15}N dipole–dipole/^{1}H^N CSA cross-correlated relaxation [28–30]. The value of δ is set to approximately $\frac{1}{2J_{HN}}$ to generate anti-phase magnetization. (B) Decay profiles of ^{1}H^N transverse magnetization of K5, D51, and G13 in a [U-^{15}N,^{2}H]-labeled protein L sample measured using the sequence in panel A at a spectrometer field of 23.5 T, 25 °C, using four different ^{15}N inversion pulses as shown. Points are experimental data with solid lines indicating best fits to an exponential decay function (exp(-R_2T), see Materials and Methods), and RMSD is the root-mean-squared deviation between the experimental and fitted data multiplied by 1000. Errors for the data points are smaller than the symbols. (C) Linear correlation plots of R_2 rates from fits of profiles generated with adiabatic pulses using all delay points (x-axis) and R_2 rates from fits of profiles with either 90°$_x$-240°$_y$-90°$_x$ (left) or 180° rectangular (middle) pulses (all points, y-axis), or R_2 values based on two data points (5 ms and 16 ms) from profiles generated using 180° rectangular pulses (right). r denotes the Pearson correlation coefficient and RMSD is the root mean square deviation between the two sets of R_2 values. Solid line is $y = x$.

composite ^{15}N pulses are used (r = 0.99, RMSD = 0.61 s^{-1}, data not shown). It is clear that either 90°$_x$-240°$_y$-90°$_x$ composite or adiabatic ^{15}N pulses are preferred in the present application, even when experiments are performed at lower magnetic fields such as 11.7 T, where artifacts are reduced but still visible (Fig. 2). There are no artifacts of this type when recording ^{1}H^N R_2 rates of the TROSY component of magnetization, as might be done in applications to large proteins, as ^{15}N pulses for refocusing cross-correlated relaxation are not applied [16] since the slowly relaxing magnetization component is desired.

In order to better understand the origin of the artifacts illustrated in Figs. 1 and 2 we have performed a series of simulations using simple spin-echo pulse schemes illustrated in the left column of Fig. 3 with ^{15}N inversion pulses that are identical to those used in the experiments (see above). Unlike the experimental case where relaxation and net evolution due to J_{HN} occur in the relaxation delay interval so as to convert in-phase to anti-phase magnetization, as discussed above (Fig. 1A), here we set δ = 0 s in Fig. 1A so as to construct the simplest possible relaxation scheme in which the starting and final magnetization is in-phase. Thus ^{15}N inversion pulses are applied at t = ¼ T and at t = ¾ T, starting with in-phase ^{1}H^N magnetization (H_x) that is assumed to be on-resonance. Decay curves were generated by calculating the magnitude of H_x at t = T. The bandwidths of the ^{15}N pulses employed in these schemes are illustrated in the middle columns of Fig. 3A-D. When focusing on the region where ^{15}N backbone chemical shifts of proteins are found, between 103 and 135 ppm, and assuming a static magnetic field of 1 GHz (corresponding to −1600 to +1600 Hz from the carrier placed at 119 ppm, Fig. 3A–D red arrows), almost perfect inversion profiles are obtained when using 90°$_x$-240°$_y$-90°$_x$ composite pulses or adiabatic pulses. In contrast, the inversion profiles are not ideal when using 180° rectangular pulses or 90°$_x$-180°$_y$-90°$_x$ composite pulses, with inversion efficiencies of approximately 87% or 90%, respectively, at ± 1600 Hz from the carrier. Using the four schemes illustrated, the decay curves of ^{1}H^N magnetization were simulated under both on-resonance (^{15}N offset of 0 Hz) and moderately off-resonance (^{15}N offset of 1000 Hz) conditions (Fig. 3A–D, right) using 22 relaxation delays ranging from 5.0 ms to 62.25 ms. When using 180° rectangular or 90°$_x$-180°$_y$-90°$_x$ composite inversion pulses the computed H_x decay profiles oscillated

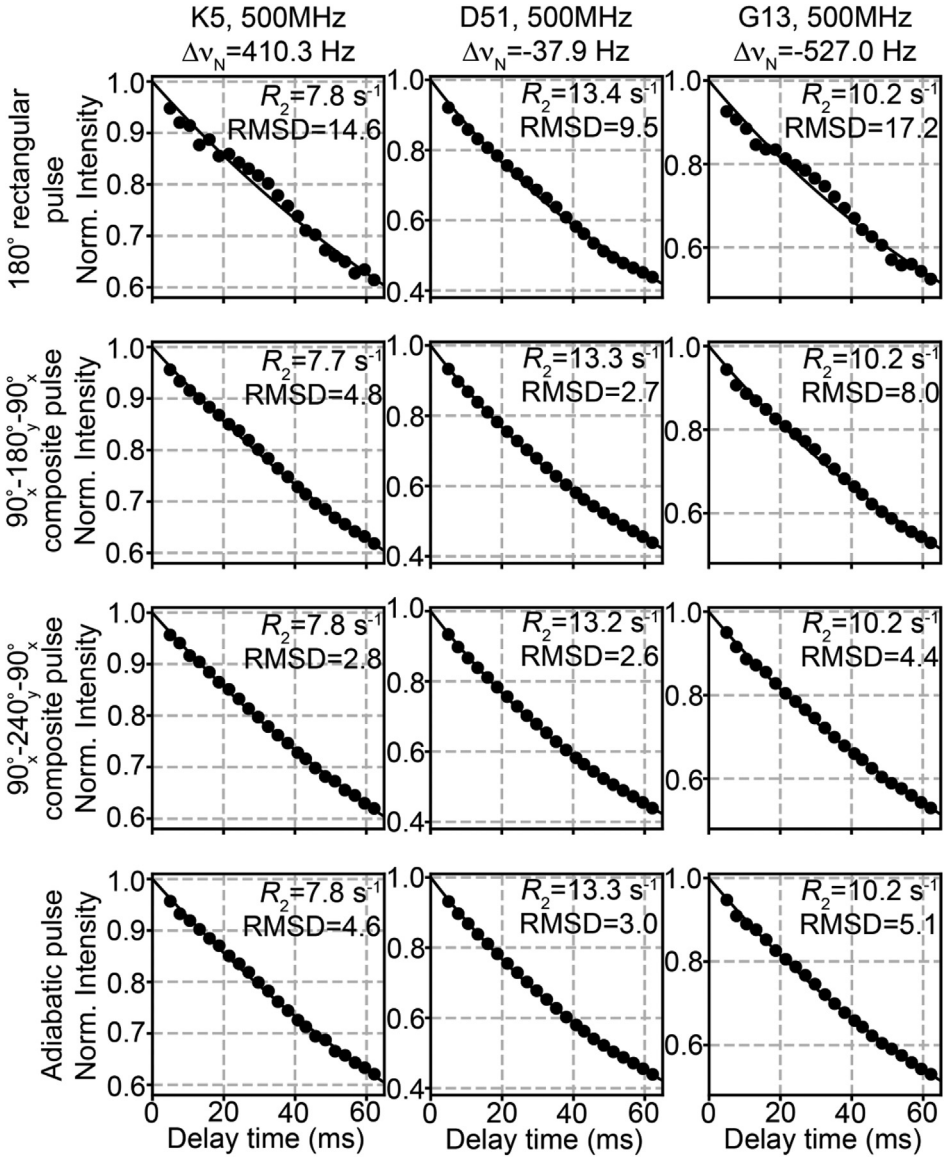

Fig. 2. Artifacts in relaxation profiles decrease at lower magnetic field. Decay profiles of ^{1}H^N magnetization of K5, D51, and G13 in a [U-^{15}N,^{2}H]-labeled protein L sample measured at a spectrometer field of 11.7 T, 25 °C. All details are as in Fig. 1, where RMSD denotes the root-mean-squared deviation between the experimental and fitted data multiplied by 1000.

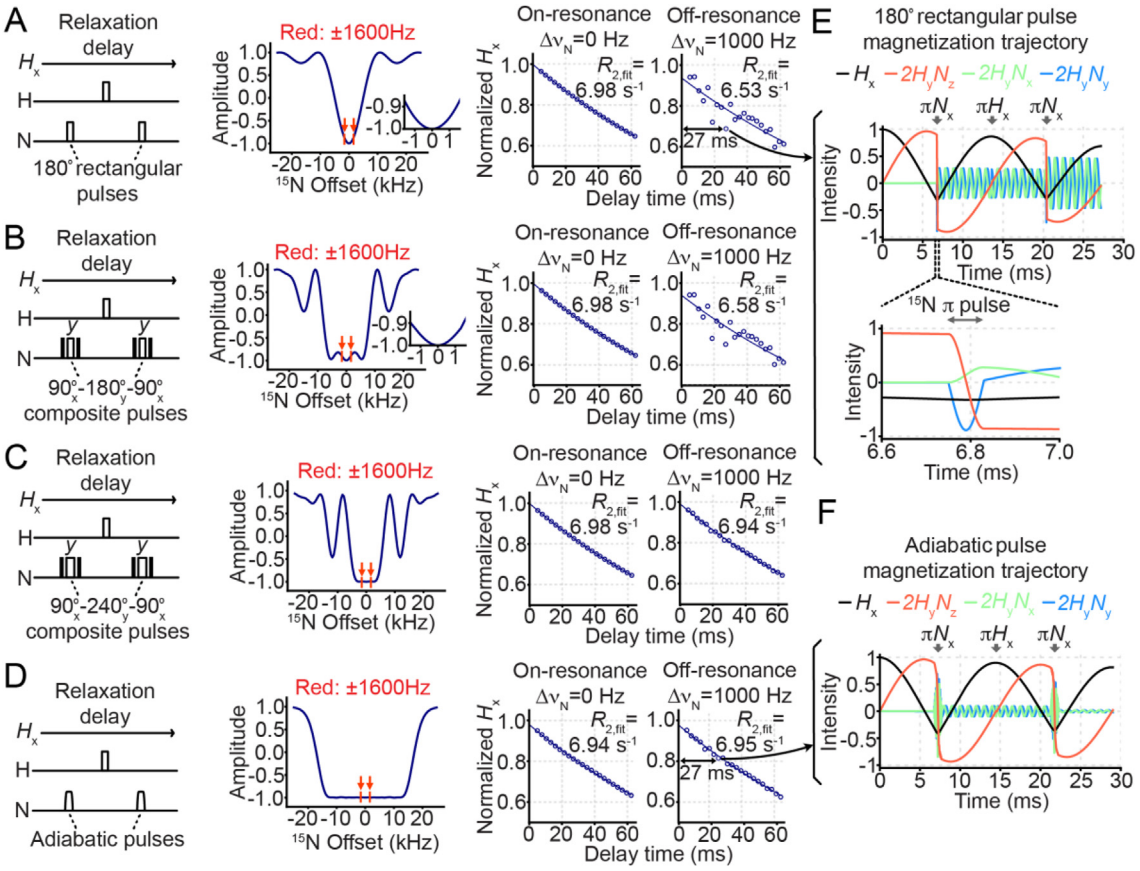

Fig. 3. Simulation of $^{1}H^{N}$ transverse magnetization decay and evolution with different ^{15}N inversion pulses. (A–D) (left) Basic pulse schemes used to simulate $^{1}H^{N}$ transverse relaxation profiles using ^{15}N 180° rectangular pulses (A), $90°_x$-$180°_y$-$90°_x$ composite pulses (B), $90°_x$-$240°_y$-$90°_x$ composite pulses (C), or adiabatic inversion pulses (D) to suppress cross-correlated spin relaxation effects. (center) Simulated bandwidths of each inversion pulse, using 6.25 kHz rectangular pulses and a 5 kHz, 1 ms duration adiabatic pulse [7]. The region corresponding to −1600 to 1600 Hz, covering the typical protein backbone ^{15}N frequency range (103–135 ppm with the carrier placed at 119 ppm at 23.5 T), is indicated by red arrows. Expanded views of this region are shown in the insets of panels A and B. (right) Simulated decay profiles of in-phase and on-resonance $^{1}H^{N}$ magnetization (H_x) as a function of relaxation delay assuming that ^{15}N pulses are either on-resonance or 1000 Hz off-resonance. Fitted relaxation rates ($R_{2,fit}$) assuming a single exponential decay are also shown in each panel. The time points calculated with a 27.0 ms relaxation delay for profiles with 180° rectangular or adiabatic pulses are highlighted, for which the evolution of the density matrix over the time course of the relaxation period was simulated in panels E and F. (E and F) The trajectory of $^{1}H^{N}$ in-phase magnetization (H_x, black), $^{1}H^{N}$-^{15}N antiphase magnetization ($2H_yN_z$, orange), and $^{1}H^{N}$-^{15}N multiple-quantum ($2H_yN_x$ and $2H_yN_y$, green and blue) coherences for a relaxation time of 27.0 ms, calculated using 180° rectangular (E) or adiabatic (F) pulses. The evolution of coherences from 6.6 ms to 7.0 ms, which includes the first ^{15}N 180° rectangular pulse, is also shown in panel E. The points at which ^{15}N or ^{1}H pulses are applied are shown as gray arrows on top of the trajectories. The intensity of each coherence is plotted along the y-axis, where the norm, $[(H_x)^2 + (2H_yN_z)^2 + (2H_yN_x)^2 + (2H_yN_y)^2]^{0.5}$, is equal to 1 (except during the 20 μs ^{1}H refocusing pulse where additional terms such $2H_zN_z$, $2H_zN_x$, and $2H_zN_y$ are created).

as a function of the relaxation delay and deviated significantly from single exponential decay functions when the pulses were applied off-resonance (Fig. 3A and B). In contrast, nearly identical, exponentially decaying curves were obtained when using $90°_x$-$240°_y$-$90°_x$ composite inversion pulses and adiabatic pulses, centered either on– or off-resonance (Fig. 3C and D). These simulations indicate that ^{15}N pulse imperfections are the source of the artifactual decay profiles observed experimentally and emphasize the importance of using pulses of sufficient bandwidth to properly invert ^{15}N magnetization. We have verified that the artifacts observed experimentally can be reproduced in simulations by computing decay profiles for K5, D51, and G13 and comparing these with the experimental profiles. Fig. S2 shows that excellent agreement is obtained.

The requirement of a near-perfect ^{15}N inversion profile is noteworthy, as both the 180° rectangular and $90°_x$-$180°_y$-$90°_x$ composite pulses invert ∼95% of ^{15}N z-magnetization at a ^{15}N offset of 1000 Hz. Thus, imperfections on the order of 5% (*i.e.*, $2H_yN_z \rightarrow -0.95\ 2H_yN_z$) are sufficient to introduce the significant artifacts observed in the decay profiles of Fig. 3A and B. Why then is the decay of $^{1}H^{N}$ magnetization so susceptible to small off-resonance effects of the ^{15}N pulses? This can be appreciated by comparing the time evolution of Cartesian product operators during the schemes illustrated in Fig. 3 using rectangular (Fig. 3E) and adiabatic (Fig. 3F) pulses for the case where $\Delta\nu_N$ = 1000 Hz. We calculated the time-evolution throughout T for a single point on the decay profiles, corresponding to a delay time of 27.0 ms, and monitored the trajectories of the four relevant components, in-phase H_x, anti-phase $2H_yN_z$, and a pair of multiple quantum (MQ) coherences, $2H_yN_x$ and $2H_yN_y$, that evolve during this interval. Starting from H_x, evolution proceeds via $^{1}H^{N}$-^{15}N scalar coupling, so that immediately prior to the first 180° rectangular ^{15}N pulse (scheme A) both in-phase and anti-phase magnetization is present via, $H_x \rightarrow H_x\cos(\pi J_{HN}\frac{T}{4}) + 2H_yN_z\sin(\pi J_{HN}\frac{T}{4})$. The majority of the anti-phase $^{1}H^{N}$ magnetization is inverted ($2H_yN_z \rightarrow -2H_yN_z$) by the ^{15}N pulse (at least 95%) but some is transferred to MQ coherences due to off-resonance effects ($2H_yN_z \rightarrow 2H_yN_x$ and $2H_yN_y$) (Fig. 3E, bottom). These MQ terms continue to evolve during the remaining portion of the relaxation delay, oscillating at their precession frequencies. Application of the second ^{15}N 180° rectangular pulse at t = $\frac{3}{4}$ T generates additional intensity for the MQ elements, transferred again from the anti-phase $2H_yN_z$ term, resulting in a signif-

icant loss of in-phase $^1H^N$ magnetization by the end of the relaxation period, which in this simulation is 27 ms (~17% loss from populating the MQ terms, neglecting relaxation). Thus, the point on the decay curve corresponding to T = 27.0 ms significantly underestimates the correct value (Fig. 3A, right). Notably, the loss of H_x varies with the different relaxation time points since the amount of anti-phase magnetization ($2H_yN_z$) at the time of the ^{15}N refocusing pulses, and hence the transfer to MQ coherences, depends on T via $\sin(\pi J_{HN}\frac{T}{4})$ (see above), leding to the oscillatory behavior observed in the H_x decay curve. For $T \sim 44$ ms ($\frac{T}{4} = \frac{1}{J_{NH}} = 11ms$) the point on the decay curve is close to the value expected for an exponential decay since there is little anti-phase magnetization at the time of the ^{15}N pulses ($2H_yN_z$ is small as $\sin(\pi J_{HN}\frac{T}{4}) \sim 0$), and therefore MQ terms are not generated. As anticipated, ^{15}N adiabatic inversion pulses generate far less MQ coherences than 180° rectangular pulses, in general, leading to near-perfect exponential decay curves, but a small amount is, nevertheless produced, even when the resonance position of the ^{15}N spin coincides with the middle of the adiabatic sweep, as has been described previously in the context of ^{13}C-^1H_n spin systems [31].

In summary, here we have revisited a simple pulse scheme for measuring $^1H^N$ transverse relaxation rates in ^{15}N labeled proteins [13]. Measured decay rates can be impacted by pulse imperfections associated with the application of ^{15}N inversion pulses to correct for small effects resulting from cross-correlated spin relaxation in cases where ^{15}N offsets are large. It is shown that near-perfect inversion of ^{15}N magnetization is required and that both ^{15}N $90°_x$-$240°_y$-$90°_x$ composite and adiabatic pulses are effective at eliminating the artifacts that would, otherwise, be present when using rectangular pulses or the common $90°_x$-$180°_y$-$90°_x$ composite pulse scheme. With the continued development of higher static magnetic fields for solution NMR applications the use of appropriate pulses becomes increasingly critical, as the present example illustrates.

Data availability statement

Python scripts for the simulations of Fig. 3 and Supporting Information Fig. S2 and for generating adiabatic refocusing pulses can be found at https://github.com/YukiToyama/Simulations_of_15N_pulse_imperfection.

Declaration of Competing Interest

The authors declare that they have no known competing financial interests or personal relationships that could have appeared to influence the work reported in this paper.

Acknowledgments

Y.T. was supported through a Japan Society for the Promotion of Science Overseas Research Fellowship, an Uehara Memorial Foundation postdoctoral fellowship, and a fellowship from the Canadian Institutes of Health Research (CIHR). A.K.R is grateful to the CIHR for post-doctoral support. This research was funded by CIHR FND-503573 and NSERC 2015-04347 grants to L.E.K.

Appendix A. Supplementary data

Supplementary data to this article can be found online at https://doi.org/10.1016/j.jmr.2023.107412.

References

[1] T.R. Alderson, L.E. Kay, NMR spectroscopy captures the essential role of dynamics in regulating biomolecular function, Cell 184 (2021) 577–595.
[2] A.R. Camacho-Zarco, V. Schnapka, S. Guseva, A. Abyzov, W. Adamski, S. Milles, M.R. Jensen, L. Zidek, N. Salvi, M. Blackledge, NMR Provides Unique Insight into the Functional Dynamics and Interactions of Intrinsically Disordered Proteins, Chem. Rev. 122 (2022) 9331–9356.
[3] J. Cavanagh, N. Skelton, W. Fairbrother, M. Rance, A. Palmer, Protein NMR Spectroscopy: Principles and Practice, Academic Press, 2006.
[4] A. Bax, S.S. Pochapsky, Optimized recording of heteronuclear multidimensional NMR spectra using pulsed field gradients, J. Magn. Reson. 99 (1992) 638–643.
[5] M. Garwood, L. DelaBarre, The return of the frequency sweep: designing adiabatic pulses for contemporary NMR, J. Magn. Reson. 153 (2001) 155–177.
[6] E. Kupce, R. Freeman, Stretched Adiabatic Pulses for Broadband Spin Inversion, J Magn Reson Series A 117 (1995) 246–256.
[7] J.M. Bohlen, G. Bodenhausen, Experimental Aspects of Chirp NMR Spectroscopy, J. Magn. Reson. Ser. A 102 (1993) 293–301.
[8] M.V. Subrahmanian, K. Pavuluri, C. Olivieri, G. Veglia, High-fidelity control of spin ensemble dynamics via artificial intelligence: from quantum computing to NMR spectroscopy and imaging PNAS Nexus 1 (2022) pgac133.
[9] Y. Xia, P. Rossi, M.V. Subrahmanian, C. Huang, T. Saleh, C. Olivieri, C.G. Kalodimos, G. Veglia, Enhancing the sensitivity of multidimensional NMR experiments by using triply-compensated pi pulses, J. Biomol. NMR 69 (2017) 237–243.
[10] B. Yu, X. Wang, J. Iwahara, Measuring Local Electrostatic Potentials Around Nucleic Acids by Paramagnetic NMR Spectroscopy, J. Phys. Chem. Lett. 13 (2022) 10025–10029.
[11] B. Yu, C.C. Pletka, B.M. Pettitt, J. Iwahara, De novo determination of near-surface electrostatic potentials by NMR, PNAS 118 (2021).
[12] B. Yu, C.C. Pletka, J. Iwahara, Protein Electrostatics Investigated through Paramagnetic NMR for Nonpolar Groups, J. Phys. Chem. B 126 (2022) 2196–2202.
[13] L.W. Donaldson, N.R. Skrynnikov, W.Y. Choy, D.R. Muhandiram, B. Sarkar, J.D. Forman-Kay, L.E. Kay, Structural characterization of proteins with an attached ATCUN motif by paramagnetic relaxation enhancement NMR spectroscopy, J. Am. Chem. Soc. 123 (2001) 9843–9847.
[14] J. Iwahara, C. Tang, G. Marius Clore, Practical aspects of ^1H transverse paramagnetic relaxation enhancement measurements on macromolecules, J. Magn. Reson. 184 (2007) 185–195.
[15] R. Ishima, P.T. Wingfield, S.J. Stahl, J.D. Kaufman, D.A. Torchia, Using Amide 1H and 15N Transverse Relaxation To Detect Millisecond Time-Scale Motions in Perdeuterated Proteins: Application to HIV-1 Protease, J. Am. Chem. Soc. 120 (1998) 10534–10542.
[16] Y. Toyama, A.K. Rangadurai, J.D. Forman-Kay, L.E. Kay, Mapping the per-residue surface electrostatic potential of CAPRIN1 along its phase-separation trajectory, Proc. Natl. Acad. Sci. U. S. A. 119 (2022).
[17] A. Mittermaier, L.E. Kay, Chi1 torsion angle dynamics in proteins from dipolar couplings, J. Am. Chem. Soc. 123 (2001) 6892–6903.
[18] F. Delaglio, S. Grzesiek, G.W. Vuister, G. Zhu, J. Pfeifer, A. Bax, NMRPipe: a multidimensional spectral processing system based on UNIX pipes, J. Biomol. NMR 6 (1995) 277–293.
[19] H. Geen, R. Freeman, Band-selective radiofrequency pulses, J. Magn. Reson. 93 (1991) 93–141.
[20] M.A. McCoy, L. Mueller, Selective decoupling, J. Magn. Reson. Ser. A 101 (1993) 122–130.
[21] S. Grzesiek, A. Bax, The importance of not saturating water in protein NMR. Application to sensitivity enhancement and NOE measurements, J. Am. Chem. Soc. 115 (1993) 12593–12594.
[22] A.J. Shaka, J. Keeler, T. Frenkiel, R. Freeman, An improved sequence for broadband decoupling: WALTZ-16, J. Magn. Reson. 52 (1983) 335–338.
[23] M.H. Levitt, R. Freeman, NMR population inversion using a composite pulse, J. Magn. Reson. 33 (1979) 473–476.
[24] R. Freeman, S.P. Kempsell, M.H. Levitt, Radiofrequency pulse sequences which compensate their own imperfections, J. Magn. Reson. 38 (1980) 453–479.
[25] P. Allard, M. Helgstrand, T. Hard, The Complete Homogeneous Master Equation for a Heteronuclear Two-Spin System in the Basis of Cartesian Product Operators, J. Magn. Reson. 134 (1998) 7–16.
[26] G. Cornilescu, A. Bax, Measurement of Proton, Nitrogen, and Carbonyl Chemical Shielding Anisotropies in a Protein Dissolved in a Dilute Liquid Crystalline Phase, J. Am. Chem. Soc. 122 (2000) 10143–10154.
[27] M. Goldman, Interference effects in the relaxation of a pair of unlike spin-12 nuclei, J. Magn. Reson. Ser. A 60 (1984) 437–452.
[28] L.E. Kay, L.K. Nicholson, F. Delaglio, A. Bax, D.A. Torchia, Pulse Sequences for Removal of the Effects of Cross Correlation between Dipolar and Chemical-Shift Anisotropy Relaxation Mechanisms on the Measurement of Heteronuclear TI and T2 Values in Proteins, J. Magn. Reson. 97 (1992) 359–375.
[29] A.G. Palmer, N. Skelton, W.J. Chazin, P.E. Wright, M. Rance, Suppression of the effects of cross-correlation between dipolar and anisotropic chemical shift relaxation mechanisms in the measurement of spin-spin relaxation rates, Mol. Phys. 75 (1992) 699–711.
[30] J. Boyd, U. Hommel, I.D. Campbell, Influence of cross-correlation between dipolar and anisotropic chemical shift relaxation mechanisms upon longitudinal relaxation rates of 15N in macromolecules, Chem. Phys. Lett. 175 (1990) 477–482.
[31] C. Zwahlen, S.J. Vincent, L.E. Kay, Analytical description of the effect of adiabatic pulses on IS, I2S, and I3S spin systems, J. Magn. Reson. 130 (1998) 169–175.